physica status solidi

pss

www.pss-journals.com

reprint

WILEY-VCH

WILEY ONLINE LIBRARY EarlyView publication on wileyonlinelibrary.com
(issue and page numbers not yet assigned;
citable using Digital Object Identifier – **DOI**)

Phys. Status Solidi A, 1–9 (2011) / **DOI** 10.1002/pssa.201127264

physica status solidi pss a
www.pss-a.com
applications and materials science

Comparison of device models for organic solar cells: Band-to-band *vs.* tail states recombination

Marcos Soldera*[,1], Kurt Taretto[1], and Thomas Kirchartz[2]

[1] Departamento de Electrotecnia, Universidad Nacional del Comahue, Buenos Aires 1400, 8300 Neuquén, Argentina
[2] Department of Physics, Imperial College London, South Kensington SW7 2AZ, UK

Received 4 May 2011, revised 25 August 2011, accepted 31 August 2011
Published online 3 October 2011

Keywords analytical models, device simulations, organic solar cells, tail states

* Corresponding author: e-mail msoldera@gmail.com, Phone/Fax: +54 299 4488305

The efficiency-limiting recombination mechanism in bulk-heterojunction (BHJ) solar cells is a current topic of investigation and debate in organic photovoltaics. In this work, we simulate state-of-the-art BHJ solar cells using two different models. The first model takes into account band-to-band recombination and field dependent carrier generation. The second model assumes a Shockley–Read–Hall (SRH) recombination mechanism via tail states and field independent carrier generation. Additionally, we include in both cases optical modelling and, thus, position-dependent exciton generation and non-ideal exciton collection. We explore both recombination mechanisms by fitting light and dark current–voltage (*JV*) characteristics of BHJ cells of five materials: P3HT, MDMO-PPV, MEH-PPV, PCDTBT and PF10TBT, all blended with fullerene derivatives. We show that although main device parameters such as short circuit current, open circuit voltage, fill factor and ideality factor are accurately reproduced by both Langevin and tail recombination, only tail recombination reproduces also the ideality factor of dark characteristics accurately. Nevertheless, the model with SRH recombination via tail states needs the inclusion of external circuitry to account for the heavy shunt present in all the blends, except P3HT:PCBM, when illuminated. Finally, we propose a means to find analytical expressions for the short circuit current by assuming a linear relation between the recombination rate and the concentration of free minority carriers. The model reproduces experimental data of P3HT cells at various thickness values using realistic parameters for this material.

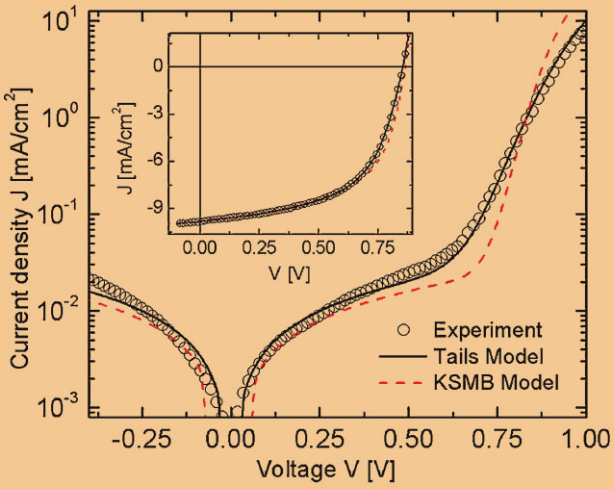

Dark *JV* measurement (circles) of a PCDTBT:$PC_{70}BM$ solar cell (Park et al., Nature Photon. **3**, 297 (2009) [1]), the fit with the model including recombination via tail states (solid line) and the fit with the model reported by (Koster et al., Phys. Rev. B **72**, 085205 (2005) [2]) that includes bimolecular band-to-band recombination and charge transfer state (CTS) dissociation. The inset shows the *JV* curves under white light.

1 Introduction Organic solar cells are currently attracting much attention in the pursuit of thin film photovoltaics due to the potential for low cost fabrication of large area modules, the mechanical flexibility and the ease of processing [3, 4]. The bulk heterojunction (BHJ) concept developed by Halls et al. [5] in 1995 represented a major breakthrough in this field by blending two organic materials, namely a donor and an acceptor, which form a heterojunction

throughout the whole active layer. This feature enhances the collection of photogenerated excitons and hence improves the power conversion efficiency (PCE), which recently reached certified 8.3% [6]. Nevertheless, this PCE is around four times smaller than the radiative efficiency limit predicted by the Shockley–Queisser theory, which can be as high as 30% if the appropriate materials are chosen [7]. This mismatch between theory and state-of-the-art cells is caused by three main loss factors, *i.e.* non-radiative recombination along the distributed heterointerfaces, inefficient collection of photogenerated excitons, and optical losses due to insufficient light trapping and parasitic absorption of the contact layers [7]. The most severe limiting factor is non-radiative recombination, which accounts for the low open circuit voltage and carrier collection.

A precise modelling of the device is required to quantify these loss mechanisms and to understand the physical processes within the device that are still being debated by the photovoltaics community, *e.g.* the mechanism of bulk and surface recombination [8–12], the influence of the active layer morphology on the device performance [13–16] and the steps towards a better light harvesting [17, 18].

Several mechanisms have been proposed and implemented in numerical models to account for bulk recombination such as monomolecular exciton decay [19], bimolecular *e.g.* Langevin-type recombination [20], trimolecular recombination and trap-assisted recombination [21, 22]. In particular, the model developed by Koster et al. [2] combines field-assisted dissociation of the charge transfer state (CTS), with Langevin-type bimolecular recombination of free carriers. This model has been widely used and has shown a good match between simulations and experimental data of BHJ cells under illumination. However, in dark current–voltage characteristics, the diode ideality factor (n_{id}) is not easily reproduced. This mismatch originates from the limitation of considering direct band recombination, which can only yield an ideality factor of unity, whereas experimental data show that typical ideality factors in BHJ cells vary between 1 and 2 [12]. This unresolved aspect pushes forward the research on a better comprehension of the dominant recombination mechanism. Recent findings have shown that the disordered nature of the organic semiconductors commonly used in BHJ cells induces exponential density of states within the forbidden gap, also known as band tail states [23–25]. A new device model [26] takes into account the recombination rate of carriers through these tail states providing a variable ideality factor between 1 and 2 [27]. This parameter can be adjusted by a suitable choice of the shape of the density of tail states and the dynamics of capture and emission of carriers into and from the localized tail states. In this work, we refine the tail recombination model by adding new features such as optical modelling and subsequently a position-dependent generation rate and finite exciton collection. This allows us to fit light as well as dark current–voltage measurements of several types of state-of-the-art BHJ cells. Finally, we present simple expressions adapted from analytical models to predict the behaviour of the short circuit current (J_{sc}) as a function of the active layer thickness (d), which can be used as a means to optimize the blend thickness.

2 Model features

2.1 Free carrier generation in BHJ solar cells Unlike inorganic semiconductors, generation of free charge carriers in organic BHJ solar cells does not stem directly from the absorption of incoming photons. On the contrary, excitons are generated, which may either decay to the ground state or diffuse, with typical diffusion lengths on the order of 10 nm. The exciton diffuses along the absorbing phase towards a heterointerface, where an ultrafast charge transfer process [28] splits the exciton into a hole in the donor, normally a fullerene derivative, and an electron in the acceptor phase, typically a conjugated polymer. This state of the split exciton is commonly referred as CTS and is the precursor for free carriers.

2.2 Exciton generation and transport We introduce a position-dependent generation rate of excitons G calculated with the transfer matrix formalism, which takes into account reflections of the solar radiation between the inner layers of the cell and interference phenomena. To account for the recombination of the optically generated excitons, we implement a finite exciton collection probability (f_χ), which is fully described in Ref. [29]. The parameter f_χ depends basically on the excitonic transport properties and on the scale of the blend morphology, yielding unity when the exciton diffusion length is much larger than the distance between two donor–acceptor interfaces.

2.3 Geminate *vs.* non-geminate recombination There has been much discussion about whether the shape of the current–voltage (JV) curve is dominated either by the voltage dependence of the CTS dissociation or by non-geminate bimolecular recombination of free carriers [11, 12, 30–32]. Recently, independent experimental tests performed by Street et al. [33] with transient photoconductivity measurements, and by Shuttle et al. [34] with charge extraction measurements, have shown that geminate CTS recombination is negligible in the materials systems poly-3-hexylthiophene:[6,6]-phenyl-C61-butyric acid methyl ester (P3HT:PCBM) and the blend based on the alternating copolymer poly[N-9″-hepta-decanyl-2,7-carbazole-alt-5,5-(4′,7′-di-2-thienyl-2′,1′,3′-benzothiadiazole) (PCDTBT) and the fullerene derivative $PC_{70}BM$. To our knowledge, there have not yet been published conclusive experimental results regarding the dominant recombination mechanisms in other types of blends like the phenylene vinylene derivatives poly[2-methoxy-5-(3′,7′-dimethyloctyloxy)-1,4-phenylene vinylene] (MDMO-PPV) blended with PCBM and poly(2-methoxy-(2′-ethyl-hexyloxy)-1,4-phenylene (MEH-PPV) blended with PCBM or poly[2,7-(9,9-dialkylfluorene)-alt-5,5-(4′,7′-di-2-thienyl-2′,1′,3′-benzothiadiazole) (PF10TBT) blended with PCBM. Therefore, we assume in our simulations with the tail states recombination

Table 1 Fit parameters of the *JV* curves reported in the references listed in each column with the tails and KSMB model (in brackets). The parameters are: electron/hole mobility $\mu_{n/p}$, exciton diffusion length L_χ, exciton collection efficiency f_χ, series resistance R_s, parallel resistance R_p, effective density of states of the conduction/valence band $N_{c/v}$, Urbach energy of the conduction and valence band E_U, the capture rates characterize the recombination of a free hole with a trapped electron in a conduction-band tail state β_p^-, the recombination of an electron with a trapped hole in the valence-band tail β_n^+, the trapping of a hole by a neutral valence-band tail state β_p^0 and the trapping of an electron by a neutral conduction-band tail state β_n^0; k_f stands for the recombination rate of the CTS. The effective band gap E_g, light power P_{photo} and blend thickness d are taken from the corresponding Refs. In the tails model the effective density of states of the tails in the conduction and valence band was set to $1.16 \times 10^{25}\,m^{-3}$ for all the fits. In the KSMB model the mean distance of the electron and hole in the CTS was fixed to 1.8 nm for all the fits. The relative dielectric constant $\varepsilon_r = 3.4$ for both models and all the simulations.

parameters	Burkhard [40] P3HT:PCBM	Mandoc [21] MDMO: PCBM	Sievers [43] MEH-PPV: PCBM	Park [1] PCDTBT: $PC_{70}BM$	Veldman [45] PF10TBT: PCBM
μ_n (m^2/Vs)	8.78×10^{-8} (3.5×10^{-7})	2.06×10^{-8} (1.3×10^{-7})	5.66×10^{-8} (8×10^{-8})	1.41×10^{-8} (1×10^{-7})	4.37×10^{-8} (1.5×10^{-7})
μ_p (m^2/Vs)	3.47×10^{-8} (3.5×10^{-8})	1.3×10^{-8} (1.3×10^{-8})	1.83×10^{-9} (8×10^{-9})	7.66×10^{-9} (1×10^{-8})	4.2×10^{-8} (1.5×10^{-8})
L_χ (nm)	5.6	4.8	11.4	12.4	13.4
f_χ (%)	80	75	94	95	91
R_s ($\Omega\,cm^2$)	0.91 (1.6)	4 (13)	0.05 (8)	1.64 (3)	9.7 (9)
R_p ($\Omega\,cm^2$)	∞	1430 (−)	4250 (−)	1330[a]–$3 \times 10^{4+}$ ($3 \times 10^{4+}$)	820[a]–$3.5 \times 10^{6+}$ ($3.5 \times 10^{6+}$)
E_U (meV)	31 (−)	95 (−)	74 (−)	79 (−)	44 (−)
$\beta_p^- = \beta_n^+$ (m^3/s)	1.81×10^{-17}	8.64×10^{-20} (−)	3.16×10^{-14} (−)	2.96×10^{-19} (−)	2.34×10^{-15} (−)
$\beta_p^0 = \beta_n^0$ (m^3/s)	5.64×10^{-17} (−)	2.88×10^{-15} (−)	2.49×10^{-18} (−)	9.35×10^{-18} (−)	2.2×10^{-18} (−)
k_f (s^{-1})	(1×10^5)	(6×10^5)	(6.5×10^5)	(4×10^5)	(2.5×10^5)
$N_c = N_v$ (m^{-3})	2.5×10^{26}	5×10^{25}	2×10^{26}	1×10^{25}	2.5×10^{25}
E_g (eV)	1.1	1.26	1.37	1.2	1.4
d (nm)	220	90	130	80	210
P_{photo} (mW/cm^2)	100	100	166	100	75

[a]Shunt under illumination, + shunt in the dark.

model that the generation rate of free carriers is independent of the electric field and thus depends only on the spatial coordinate and the exciton collection efficiency.

2.4 Recombination via tail states The recombination rate of free carriers via band tail states used in our simulations follows from Shockley–Read–Hall (SRH) statistics [35, 36], which assumes band–tail transitions where at least one free carrier is available. In other words, trapped electrons are not allowed to recombine with trapped holes. Therefore, the possible transitions imply either a free carrier recombining with a carrier of the opposite charge trapped in a tail state or the capture of a carrier by an unoccupied tail state. Each of these transitions is characterized by a capture rate coefficient. The band tails are defined by their characteristic Urbach energy and density of tail states at the band edges. For a full description see Ref. [26].

3 Application to experimental data

3.1 *JV* curves fitting In order to prove the consistency of the tails model we performed fits of BHJ cells prepared and measured by different research groups. For each *JV* curve we also show, for the sake of comparison, the corresponding fit realized with the model that takes into account field-assisted dissociation of the CTS and Langevin recombination [2], from now on called KSMB model after the authors of Ref. [2]. Additionally, we used in the KSMB model a position-dependent exciton generation rate combined with a finite exciton collection as calculated in the tails model, with the purpose of comparing both models from the basis of having the same rate of CTS generation. All the parameters used for the fits in this section are listed in Table 1.

The P3HT:PCBM (1:1) system is one of the most intensively studied materials in the organic photovoltaics field with PCEs up to 5% [37–39]. Both models reproduce accurately the *JV* curve measured by Burkhard [40] as shown in Fig. 1. As expected, external circuitry is not needed to reproduce the shape of the *JV* curve at low bias. According to Table 1, the *JV* fits to the P3HT:PCBM data yield parameter values that are close to those found in the literature. The Urbach energy extracted from the fit is $E_U = 31$ meV, which is close to the value $E_U = 37$ meV obtained by Street et al. [24] using photoconductivity spectral measurements and such values are on the order of the results of Rivnay et al. [25] using density functional theory calculations. The electron and hole mobilities obtained from the fit are on the order of the measurements performed by Mihailetchi et al. [41] who obtained the values $\mu_n = 3 \times 10^{-7}\,m^2/Vs$ and $\mu_p = 2 \times 10^{-8}\,m^2/Vs$ from the space-charge limited current measured using an electron- and hole-only device configuration. Since this model includes excitonic transport, we are

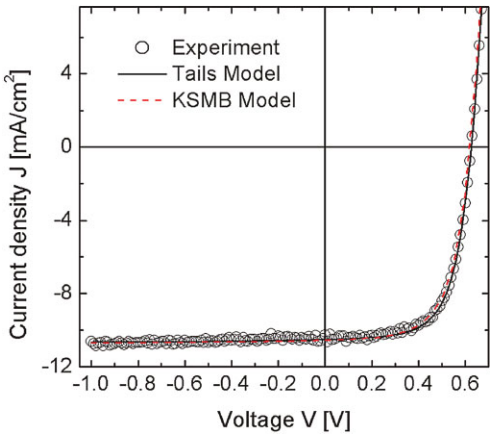

Figure 1 (online colour at: www.pss-a.com) Current–voltage characteristics of a P3HT:PCBM [40] cell under white light 100 mW/cm^2 illumination and the fits with the model including tails and the KSMB model.

able to use the exciton diffusion length L_χ as a fitting parameter of the *JV* data. Particularly, we obtain $L_\chi = 5.6$ nm for this polymer. To our knowledge, measurements of L_χ in this type of blend have not been done yet, nevertheless Kroeze et al. [42] measured an L_χ between 2 and 5 nm on a pure P3HT film deposited on top of anatase TiO_2 layer using the flash-photolysis time-resolved microwave conductivity technique.

Solar cells based on the phenylene vinylene derivatives MDMO-PPV and MEH-PPV were also well reproduced with the model, as shown in Fig. 2, where the experimental data were taken from Refs. [21] and [43], respectively. Unlike the simulations of P3HT:PCBM cells, these simulations need the inclusion of an external parallel resistor to account for the heavy voltage dependence at reverse and low forward bias. On the other hand, the simulations with the KSMB model do not require an external shunt, because the field-assisted dissociation of the CTS described by the Onsager–Braun theory dominates the shape in this part of the *JV* curve.

To further demonstrate the influence of the applied voltage on the dissociation efficiency of the CTS in these blends, we show in Fig. 3 the calculated dissociation probability (P_{dis}) as a function of the applied voltage for the MDMO-PPV:PCBM cell, with $d = 90$ nm and $E_g = 1.26$ eV, and for the P3HT:PCBM device, with $d = 220$ nm and $E_g = 1.1$ eV, using the Onsager–Braun theory with the model parameters outlined in Table 1. As expected, the MDMO-PPV:PCBM device shows a strong dependence on the applied voltage and therefore we assume that geminate recombination plays an important role at low bias. On the other hand, the P3HT:PCBM device is nearly bias independent at low and reverse bias, and thus geminate recombination can be neglected. This assertion agrees with the experimental results of Refs. [33, 34] and with the simulations performed by Tumbleston et al. [44].

So far, our results show that both Langevin and tail-recombination seem to be able to reproduce illuminated *JV* characteristics. In the case of the phenylene vinylene-based blends the tails model can only adjust accurately the *JV* curves if a shunt is included to account for the slope close to short circuit conditions. In the following, we show that only tail recombination reproduces dark as well as light *JV* curves simultaneously, and in the studied cases this device model simulates the diode behaviour more accurately than the KSMB model independently of resistive effects.

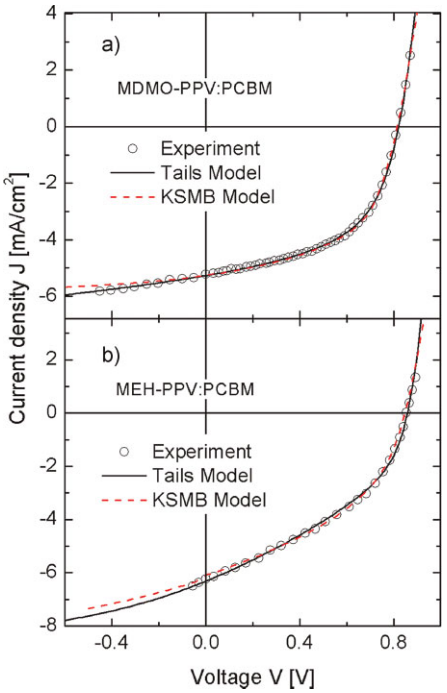

Figure 2 (online colour at: www.pss-a.com) Current–voltage characteristics of (a) a MDMO-PPV:PCBM cell measured by Mandoc et al. [21] and (b) a MEH-PPV:PCBM measured by Sievers et al. [43] and the fits with the model including tails and the KSMB model.

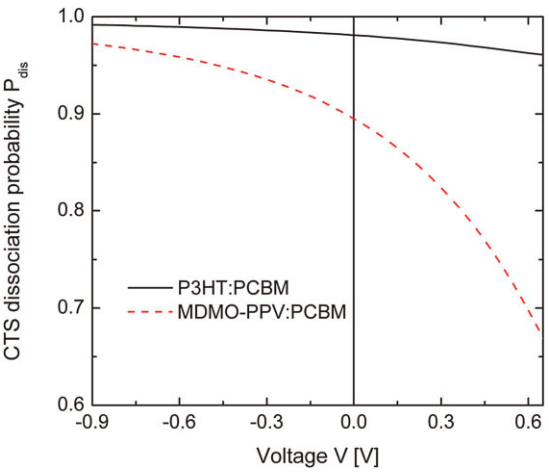

Figure 3 (online colour at: www.pss-a.com) Dissociation probability of the CTS as a function of the applied voltage for two different materials systems. The simulation parameters are the same as in the simulations with the KSMB model of Figs. 1 and 2a.

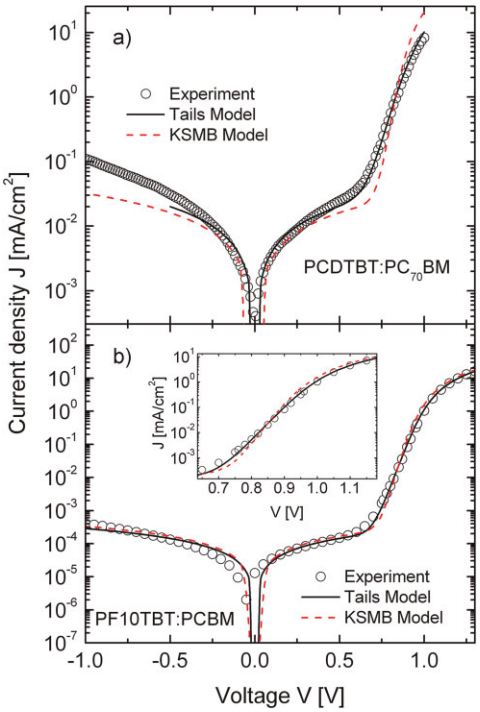

Figure 4 (online colour at: www.pss-a.com) Dark current–voltage measurements taken from Refs. [1] (a) and [45] (b), the fits with the tails model and the KSMB model. The inset shows in detail the region where the dark ideality factor can be extracted.

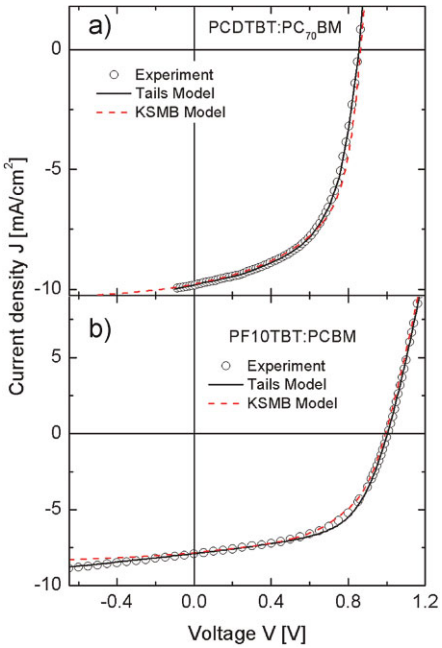

Figure 5 (online colour at: www.pss-a.com) Current–voltage characteristics of (a) PCDTBT:PC70BM cell measured by Ref. [1] under white light 100 mW/cm^2 illumination and (b) PF10TBT:PCBM cell from Ref. [45] under white light 75 mW/cm^2 illumination. The lines are fits with the model including tails and the KSMB model.

In order to illustrate the potential of the tails model to reproduce the dark ideality factor, we show in Fig. 4 fits for two different materials systems measured by the authors of Refs. [1] and [45], namely (a) the blend based on the alternating co-polymer PCDTBT:$PC_{70}BM$ with $n_{id} = 2.1$ and (b) the benzothiadiazole-containing blend PF10TBT:PCBM with $n_{id} = 1.4$, respectively. The trade-off between accurately fitting the dark and light (shown below) *JV* curves with the same model parameters yields an optimum $n_{id} = 2$ in the PCDTBT:$PC_{70}BM$ cell and $n_{id} = 1.36$ in the PF10TBT:PCBM cell. In both cases the KSMB model provides a unique ideality factor of unity. The simulations in the dark require a shunt to account for the shoulder at low forward bias, where the diode behaviour is screened.

The saturation current density of the diode (J_0) can be extracted from the *y*-axis intercept of the linear fit of the dark log(*J*) *vs*. *V* (Fig. 4). In the PCDTBT:$PC_{70}BM$ /PF10TBT:PCBM cells the extracted values are $J_0 = 4.9 \times 10^{-7}$/2.5×10^{-12} mA/cm^2, which are much smaller than the reverse current in both devices observed in Fig. 4, suggesting that a strong shunt must dominate the reverse current. Our fits for the PCDTBT:$PC_{70}BM$/PF10TBT:PCBM device yielded Ohmic shunts $R_p = 3 \times 10^4/3.5 \times 10^6\ \Omega\,\text{cm}^2$, and therefore, the simple electrical model predicts reverse currents, for instance at -1 V, of $J(-1\text{ V}) = 3.3 \times 10^{-2}/2.9 \times 10^{-4}$ mA/cm^2. In the case of the PF10TBT:PCBM cell, the magnitude and shape of the measurements can be followed by both tails and KSMB models, but the data reported for the PCDTBT:$PC_{70}BM$ device present a non-Ohmic shunt which cannot be accurately reproduced with the models considered in this work.

Figure 5 shows the fits of the experimental data under illumination using the same model parameters as in the simulations in the dark (Fig. 4). Again, both models explain satisfactorily the illuminated characteristics of the cells. In the case of the KSMB model, the values of the external shunts were kept the same as in the dark, but in the tails models the shunts must be much smaller (see Table 1) than their dark counterpart to accurately fit the *JV* curve near short circuit conditions. We suggest that the non-linear shunts depend on the illumination intensity and on the high electric field present under reverse bias. Further investigations on the recombination mechanisms in this regime are needed to clarify the reverse current dependence in the dark as well as under illumination.

3.2 Carrier lifetime Recombination dynamics in BHJ cells can be characterized by the carrier lifetime τ, which depends on multiple factors such as the dominant recombination mechanism, bias and illumination intensity. Several studies report the experimental determination of τ in BHJ cells using different techniques and under different bias and illumination conditions [46–52]. Among them, transient photovoltage decay method TPV [52] provides the advantage to analyse the steady state lifetime under continuous irradiation, *i.e*. close to device operation regime,

and at open circuit conditions V_{oc}, where the recombination plays a crucial role. The authors of Ref. [52] report that τ follows an exponential law according to $\tau = \exp(-\beta V_{oc})$, which can be measured by varying the incident light power. Moreover, they arrived at the conclusion that the carrier lifetime depends on injection, following an inverse relationship as the charge concentration increases. Transient photovoltage experiments are in agreement with impedance spectroscopy results on P3HT:PCBM cells.

Next, we calculate the lifetime simulating a P3HT:PCBM cell using the tails model and the band-to-band recombination. The carrier lifetime can be defined as the quotient between the excess minority carrier concentration and the recombination rate [53], which in average yields

$$\tau = \frac{\overline{\Delta n}}{\overline{R}} = \int_0^d (n_f + n_t - n_{f0} - n_{t0})\mathrm{d}x \Big/ \int_0^d R\mathrm{d}x, \qquad (1)$$

where n_f and n_t are the free and trapped electron concentration and where the subscript 0 stands for thermodynamic equilibrium. In the case of the model including only band-to-band recombination, the definition of τ remains with the restriction $n_t = n_{t0} = 0$, and setting R as the Langevin recombination rate. As we show below, the values of τ as defined by Eq. (1) depend on the working conditions of the device.

Figure 6 shows the lifetime calculated with Eq. (1) under open circuit (oc) and short circuit (sc) conditions, as well as experimental results using TPV, which also belong to the open circuit situation. The closed circles represent τ calculated using recombination through tail states, and the open circles indicate τ obtained with direct band recombination. The parameters used in both models are $E_g = qV_{bi} = 1.1$ eV, $d = 120$ nm, $\varepsilon_r = 3.4$, $\mu = \mu_p = \mu_n = 7.7 \times 10^{-8}$ m^2/Vs, $N_{cv} = N_c = N_v = 2.5 \times 10^{26}$ m^{-3}, $f_\chi = 0.95$ and $R_s = 1\,\Omega$ cm^2, the simulation parameters for the tails model are $E_U = 50$ meV, and $\beta = \beta_b^0 = \beta_p^0 = \beta_n^0 = \beta_p^- = \beta_n^+ = 8 \times 10^{-17}$ m^3/s, and the parameters of the direct band recombination model are $k_f = 4 \times 10^5$ s^{-1}, and $a = 1.8$ nm. The simulated light spectrum corresponds to the standard AM1.5G, with varying values of P_{photo}, for instance 10, 100 and 1000 W/m^2. The closed stars are experimental lifetimes obtained under small perturbation excitation [52], and the open stars are the experimental results obtained under large perturbation excitation [54]. Thus, our simulations show that at open circuit both recombination mechanisms describe a steep decrease in τ as P_{photo} increases, in a manner similar to the TPV experiments. Notice that the magnitudes of the calculated lifetimes are in agreement with the experimental values.

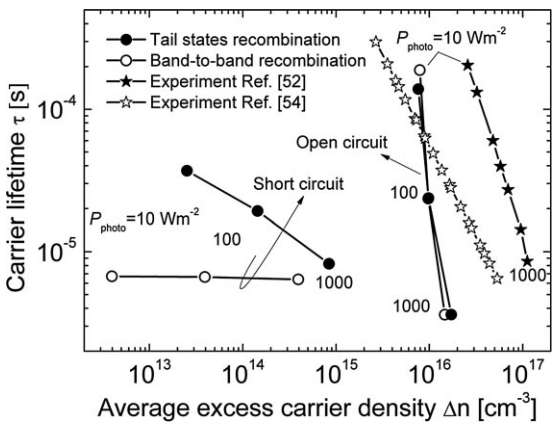

Figure 6 Carrier lifetime on a P3HT:PCBM cell as defined in Eq. (1), calculated with recombination through tail states (closed circles) and direct band recombination (open circles). The incident light power is indicated next to the simulation points. The closed and open stars are the measured lifetimes after Ref. [52] and [54], respectively.

At this point, it is important to make clear the distinction between the carrier lifetime at oc and sc. While the former is defined as a solely recombination parameter, the latter accounts also for the carriers density decrease due to the extraction current. Thus, the lifetime at sc defined with Eq. (1) should be understood as a characteristic device parameter rather than a pure material parameter. As shown below, this distinction leads to different values of τ between short circuit and open circuit conditions, for both recombination models. While band-to-band recombination gives a constant lifetime for the studied range of P_{photo}, τ calculated with the tails model decreases nearly an order of magnitude when P_{photo} decreases two orders. The predicted values of τ at sc are not necessarily higher than the oc lifetimes, since we are considering different device operation conditions. For instance, at 1-sun illumination τ at sc is larger than at oc, while the opposite holds for $P_{photo} < 100$ W/m^2.

4 Short circuit current *vs.* thickness dependence From the design point of view, it is of great importance to determine the optimum active layer thickness, which is a trade-off between optical absorption and efficient carrier transport. Since the thickness of each layer of the stack is on the order of the wavelength of incoming radiation, interference effects appear throughout the multilayer system, affecting the exciton generation profile in the active layer. Therefore, an increase in the absorber thickness does not necessarily enhance the absorption of incident photons. For that reason, an expression to predict the short circuit current (J_{sc}) as a function of d must include a generation rate calculated with a thin film optics formalism [18]. On the other hand, increasing d does at all times reduce the carrier collection efficiency due to an increase in the distance the carriers must drift and diffuse, and due to a decrease in the built-in electric field at a given built-in voltage.

The charge transport in organic BHJ cells and conventional *pin* cells relies on the same device architecture, namely a built-in electric field along the absorber, which facilitates the extraction of low mobility carriers. Since several analytical models have been proposed to describe the *JV* characteristics of inorganic *pin* type diodes and solar cells

[55–59], it is reasonable to apply them to BHJ cells taking into account the particularities of the organic semiconductors. Next, we adapt two of these models to BHJ cells with exponential density of states in the mobility gap.

4.1 Linearization of the recombination rate Analytical expressions of current–voltage characteristics based on the mobility-lifetime product ($\mu\tau$) are mathematically accessible through the assumption of a linear relation between the free carrier concentration and carrier lifetime. In a semiconductor with exponential tail states within the forbidden band, it is possible to describe the recombination rate by the expression [60]

$$R = \beta_{\mathrm{p}}^{-} n_{\mathrm{t}} p + \beta_{\mathrm{n}}^{+} p_{\mathrm{t}} n, \tag{2}$$

where $\beta_{\mathrm{p}}^{-}/\beta_{\mathrm{n}}^{+}$ are the rates at which free holes/electrons are captured by electrons/holes trapped in the conduction/valence band, n/p are the densities of free electrons/holes and $n_{\mathrm{t}}/p_{\mathrm{t}}$ are the densities of the trapped electrons/holes in the mobility gap. Then, assuming as a first order approximation under short-circuit conditions, that the concentrations of trapped electrons/holes are constant in the regions where the free holes/electrons are minority carriers, the recombination rate from Eq. (2) can be written as

$$R \cong \begin{cases} \dfrac{p}{\tau_{\mathrm{p}}} & \text{if } p < n \\ \dfrac{n}{\tau_{\mathrm{n}}} & \text{if } n < p, \end{cases} \tag{3}$$

where $\tau_{\mathrm{p}}/\tau_{\mathrm{n}}$ are the lifetimes of holes/electrons. This assumption is in agreement with our simulations with the full numerical model with tails. The piecewise linear recombination rate expressed by Eq. (3), together with the assumption that the built-in field is constant along the whole active layer and given by the work function difference of the contacts, permits us to use the mentioned analytical models to obtain first-order approximations of J_{sc} under tail states recombination.

4.2 Drift current model Merten et al. [57] developed an analytical model for a-Si *pin* cells, whose main assumptions are that diffusion currents are neglected, and the electric field in the absorber is constant and large, which is the case at short-circuit and reverse voltages in thin devices. The short circuit current is then given by

$$J_{\mathrm{scM}} = J_{\mathrm{max}} \left(1 - \frac{d^2}{(\mu\tau)_{\mathrm{eff}} (V_{\mathrm{bi}} + J_{\mathrm{scM}} R_{\mathrm{s}})} + \frac{J_{\mathrm{scM}} R_{\mathrm{s}}}{R_{\mathrm{p}}} \right), \tag{4}$$

where we define $J_{\mathrm{max}} = q G_{\mathrm{mean}} f_{\chi} d$ as the maximum attainable photocurrent in an organic BHJ cell with perfect free carrier collection and finite exciton collection f_{χ}. G_{mean} is the spatial average of the exciton generation rate and q the elementary charge. The built in potential V_{bi} together with the resistive potential drop $J_{\mathrm{scM}} R_{\mathrm{s}}$ determine the internal electric field. In our simulations of P3HT:PCBM cells, the last term is neglected since the shunt resistance R_{p} is several orders of magnitude larger than the series resistance R_{s} for the studied P3HT:PCBM solar cells.

4.3 Drift-diffusion current model In Ref. [58], a further improvement to the drift model was implemented by considering both drift and diffusion currents. The authors arrived at a closed form expression for the current–voltage relation in *pin* cells and, particularly, they validated the results for nano and microcrystalline silicon *pin* cells. The main assumptions comprise a constant electric field, flat quasi-Fermi levels in the regions where the corresponding carriers are majority and equal mobility-lifetime products for electrons and holes. The analytical expression for the short circuit current is given by

$$J_{\mathrm{scT}} = J_{\mathrm{max}} \frac{e^{\xi/2} - 1}{\xi/2}, \tag{5}$$

with

$$\xi = \frac{V_{\mathrm{bi}} - J_{\mathrm{scT}} R_{\mathrm{s}}}{2V_{\mathrm{t}}} - \sqrt{\left(\frac{d}{L}\right)^2 + \left(\frac{V_{\mathrm{bi}} - J_{\mathrm{scT}} R_{\mathrm{s}}}{2V_{\mathrm{t}}}\right)^2}, \tag{6}$$

where L is the diffusion length of minority carriers which can be calculated with the Einstein relation $L = (V_{\mathrm{t}}\mu\tau)^{1/2}$, where V_{t} is the thermal voltage.

4.4 Application to experimental data Here, we compare the numerical and analytical simulations with the data reported by Monestier et al. [61], who measured the short circuit current as a function of absorber thickness in P3HT:PCBM cells. Figure 7 shows the experimental data (open circles), the numerical simulation with the tails model (solid line), the analytical approaches (dashed lines) and the maximum attainable photocurrent J_{max} (dotted line). We first fitted the measurements with the full numerical model (solid line in Fig. 7) for a blend thickness of 75 nm and then kept all the fitting parameters and repeated the simulations over the analysed range of d. In all these simulations we assumed symmetric lifetimes and mobilities for simplicity. The parameters used in the numerical simulations are $E_{\mathrm{g}} = qV_{\mathrm{bi}} = 1.1\,\mathrm{eV}$, $\mu = \mu_{\mathrm{p}} = \mu_{\mathrm{n}} = 7.7 \times 10^{-8}\,\mathrm{m^2/Vs}$, $\beta = \beta_{\mathrm{p}}^{0} = \beta_{\mathrm{n}}^{0} = \beta_{\mathrm{p}}^{-} = \beta_{\mathrm{n}}^{+} = 8 \times 10^{-17}\,\mathrm{m^3/s}$, $N_{\mathrm{cv}} = N_{\mathrm{c}} = N_{\mathrm{v}} = 2.5 \times 10^{26}\,\mathrm{m^{-3}}$, $E_{\mathrm{U}} = 50\,\mathrm{meV}$, $R_{\mathrm{s}} = 1\,\Omega\,\mathrm{cm^2}$ and $f_{\chi} = 0.95$. The analytical curves use the same values of μ, V_{bi}, f_{χ} and R_{s} as the numerical fit, and take τ as the only free parameter. The obtained lifetimes are $\tau = \tau_{\mathrm{p}} = \tau_{\mathrm{n}} = 6.5\,\mu\mathrm{s}$ in the drift model and $\tau = 1.5\,\mu\mathrm{s}$ in the drift-diffusion approach. Notice that, although the lifetimes defined in Section 3.2 depend on carrier generation/extraction conditions, the values shown in Fig. 6 at short-circuit conditions and under 1-sun illumination of about 8 μs agree with the values obtained here.

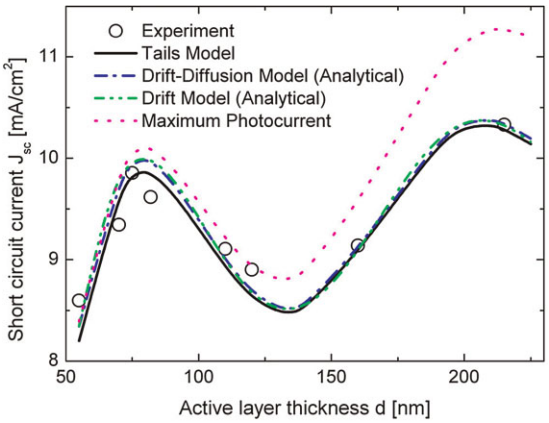

Figure 7 (online colour at: www.pss-a.com) Experimental short circuit current as a function of the blend thickness obtained by Monestier et al. [61] (open circles), the fits with the tails model (solid line), the analytical drift-diffusion model (dash dot), the analytical drift model (dash dot dot) and the maximum attainable photocurrent in BHJ cells (dot).

Despite their simplicity, we notice that the analytical approaches are able to explain the thickness dependence of J_{sc}, provided the photogeneration rate is calculated *a priori* for each thickness.

The difference between the values of the lifetime resulting from the analytical approaches is explained as follows. In the case of the model that takes into account drift and diffusion, both mechanisms are additive and contribute to the photocurrent, therefore a smaller lifetime suffices to reach the same photocurrent that is obtained with the drift model.

We performed a lifetime sensitivity analysis of the analytical models and found that the short circuit currents calculated with both models take similar values when the lifetimes change in the same proportion. In the range of blend thickness d between 50 and 150 nm there is little room for a current increase with lifetime because J_{max} is only 5% larger than the results of both analytical models and experiments. In the range $d = 150$–225 nm, however, J_{max} is up to 10% larger than the device simulations with the extracted lifetimes. If we multiply τ by a factor 2, J_{sc} increases by 4%, whereas when using a multiplicator of 10, J_{sc} increases by near 10%, matching J_{max}. On the other hand, when τ is reduced 50%, we find that J_{sc} decreases less than 5% in the interval $d =$ 50–150 nm and less than 10% in the range $d = 150$–225 nm.

5 Conclusions In this work, we discussed the validity of assuming a recombination rate via tail states in BHJ cells and compared the results to the widely used band-to-band recombination rate. We applied the model to cells based on five different active layer materials and obtained in all the studied cases highly satisfactory fits of *JV* measurements under illumination and in the dark. Particularly, the flexibility of the tails model to adjust the ideality factor between 1 and 2, seems essential to fit *JV* curves of different blends. On the other hand, the model that takes into account bimolecular Langevin-type recombination has the intrinsic drawback of providing a unique ideality factor of unity, which is a characteristic of direct band recombination.

Our simulations and results of P3HT:PCBM cells are in agreement with the literature, in the sense that field-assisted dissociation is not required to reproduce the shape of the *JV* curve. Furthermore, the dependence of the lifetime at open circuit conditions is coherent with the experimental results reported in the literature using the transient photovoltage technique. On the other hand, geminate recombination could be a valid mechanism to explain the strong voltage dependence of the *JV* curve at low bias in the other blends analysed in this work.

The dependence of the short circuit current of a P3HT:PCBM cell with the blend thickness was modelled with two different analytical expressions developed for inorganic *pin* cells and contrasted to experimental measurements and to the full numerical model using tail state recombination. The parameters that reproduce the data are realistic for this material, yielding lifetimes in the μs range. Even though the analytical expressions can be utilized as simple tools to estimate the blend thickness at which the photocurrent is maximized, it is worth noting that the generation profile must be first calculated using a thin film optics formalism to account for the influence of interferences on the $J_{sc}(d)$ characteristics.

Acknowledgements The authors would like to thank G. Burkhard (Stanford University) and S. Meskers (TU Eindhoven) for kindly providing *JV* data, and U. Rau (Forschungszentrum Jülich) for continuous support. T.K. acknowledges support by an Imperial College Junior Research Fellowship.

References

[1] S. H. Park, A. Roy, S. Beaupre, S. Cho, N. Coates, J. S. Moon, D. Moses, M. Leclerc, K. Lee, and A. J. Heeger, Nature Photon. **3**, 297 (2009).
[2] L. J. A. Koster, E. C. P. Smits, V. D. Mihailetchi, and P. W. M. Blom, Phys. Rev. B **72**, 085205 (2005).
[3] C. J. Brabec and J. R. Durrant, MRS Bull. **33**, 670 (2008).
[4] F. C. Krebs, Sol. Energ. Mater. Sol. Cells **93**, 394 (2009).
[5] J. J. M. Halls, C. A. Walsh, N. C. Greenham, E. A. Marseglia, R. H. Friend, S. C. Moratti, and A. B. Holmes, Nature **376**, 498 (1995).
[6] M. A. Green, K. Emery, Y. Hishikawa, and W. Warta, Prog. Photovoltaics Res. Appl. **19**, 84 (2011).
[7] T. Kirchartz, K. Taretto, and U. Rau, J. Phys. Chem. C **113**, 17958 (2009).
[8] C. Groves and N. C. Greenham, Phys. Rev. B **78**, 155205 (2008).
[9] C. Deibel, A. Wagenpfahl, and V. Dyakonov, Phys. Status Solidi RRL **2**, 175 (2008).
[10] T. Kirchartz, B. E. Pieters, K. Taretto, and U. Rau, Phys. Rev. B **80**, 035334 (2009).
[11] C. Deibel and A. Wagenpfahl, Phys. Rev. B **82**, 207301 (2010).

[12] R. A. Street, M. Schoendorf, A. Roy, and J. H. Lee, Phys. Rev. B **81**, 205307 (2010).
[13] X. Yang, J. Loos, S. C. Veenstra, W. J. H. Verhees, M. M. Wienk, J. M. Kroon, M. A. J. Michels, and R. A. J. Janssen, Nano Lett. **5**, 579 (2005).
[14] P. Vanlaeke, A. Swinnen, I. Haeldermans, G. Vanhoyland, T. Aernouts, D. Cheyns, C. Deibel, J. D'Haen, P. Heremans, J. Poortmans, and J. V. Manca, Sol. Energy Mater. Sol. Cells **90**, 2150 (2006).
[15] A. Alexeev, J. Loos, and M. M. Koetse, Ultramicroscopy **106**, 191 (2006).
[16] X. Yang, J. K. J. van Duren, R. A. J. Janssen, M. A. J. Michels, and J. Loos, Macromolecules **37**, 2151 (2004).
[17] J. Y. Kim, S. H. Kim, H.-H. Lee, K. Lee, W. Ma, X. Gong, and A. J. Heeger, Adv. Mater. **18**, 572 (2006).
[18] L. A. A. Pettersson, L. S. Roman, and O. Inganas, J. Appl. Phys. **86**, 487 (1999).
[19] M. Burgelman and B. Minnaert, Thin Solid Films **511/512**, 214 (2006).
[20] L. J. A. Koster, V. D. Mihailetchi, and P. W. M. Blom, Appl. Phys. Lett. **88**, 093511 (2006).
[21] M. M. Mandoc, F. B. Kooistra, J. C. Hummelen, B. de Boer, and P. W. M. Blom, Appl. Phys. Lett. **91**, 263505 (2007).
[22] N. C. Giebink, G. P. Wiederrecht, M. R. Wasielewski, and S. R. Forrest, Phys. Rev. B **82**, 155305 (2010).
[23] G. Garcia-Belmonte and J. Bisquert, Appl. Phys. Lett. **96**, 113301 (2010).
[24] R. A. Street, K. W. Song, J. E. Northrup, and S. Cowan, Phys. Rev. B **83**, 165207 (2011).
[25] J. Rivnay, R. Noriega, J. E. Northrup, R. J. Kline, M. F. Toney, and A. Salleo, Phys. Rev. B **83**, 121306 (2011).
[26] T. Kirchartz, B. E. Pieters, J. Kirkpatrick, U. Rau, and J. Nelson, Phys. Rev. B **83**, 115209 (2011).
[27] C. van Berkel, M. J. Powell, A. R. Franklin, and I. D. French, J. Appl. Phys. **73**, 5264 (1993).
[28] C. J. Brabec, N. S. Sariciftci, and J. C. Hummelen, Adv. Funct. Mater. **11**, 15 (2001).
[29] T. Kirchartz, B. E. Pieters, K. Taretto, and U. Rau, J. Appl. Phys. **104**, 094513 (2008).
[30] R. A. Street, Phys. Rev. B **82**, 207302 (2010).
[31] C. Deibel, T. Strobel, and V. Dyakonov, Adv. Mater. **22**, 4097 (2010).
[32] T. M. Clarke and J. R. Durrant, Chem. Rev. **110**, 6736–6767 (2010).
[33] R. A. Street, S. Cowan, and A. J. Heeger, Phys. Rev. B **82**, 121301 (2010).
[34] C. G. Shuttle, R. Hamilton, B. C. O'Regan, J. Nelson, and J. R. Durrant, Proc. Natl. Acad. Sci. USA **107**, 16448 (2010).
[35] W. Shockley and W. T. Read, Phys. Rev. **87**, 835 (1952).
[36] R. N. Hall, Phys. Rev. **87**, 387 (1952).
[37] Y. Kim, S. Cook, S. Tuladhar, S. Choulis, J. Nelson, J. Durrant, D. Bradley, M. Giles, I. McCulloch, C.-S. Ha, and M. Ree, Nature Mater. **5**, 197 (2006).
[38] G. Li, V. Shrotriya, Y. Yao, and Y. Yang, J. Appl. Phys. **98**, 043704 (2005).
[39] G. Dennler, M. C. Scharber, and C. J. Brabec, Adv. Mater. **21**, 1323 (2009).
[40] G. F. Burkhard, Standford University, Internal Communication.
[41] V. D. Mihailetchi, H. X. Xie, B. de Boer, L. J. A. Koster, and P. W. M. Blom, Adv. Funct. Mater. **16**, 699 (2006).
[42] J. E. Kroeze, T. J. Savenije, M. J. W. Vermeulen, and J. M. Warman, J. Phys. Chem. B **107**, 7696 (2003).
[43] D. W. Sievers, V. Shrotriya, and Y. Yang, J. Appl. Phys. **100**, 114509 (2006).
[44] J. R. Tumbleston, D.-H. Ko, E. T. Samulski, and R. Lopez, J. Appl. Phys. **108**, 084514 (2010).
[45] D. Veldman, O. İpek, S. C. J. Meskers, J. Sweelssen, M. M. Koetse, S. C. Veenstra, J. M. Kroon, S. S. van Bavel, J. Loos, and R. A. J. Janssen, J. Am. Chem. Soc. **130**, 7721–7735 (2008).
[46] A. Pivrikas, N. S. Sariciftci, G. Juška, and R. Österbacka, Prog. Photovoltaics Res. Appl. **15**, 677 (2007).
[47] G. Dennler, A. J. Mozer, G. Juska, A. Pivrikas, R. Österbacka, A. Fuchsbauer, and N. S. Sariciftci, Org. Electron. **7**, 229 (2006).
[48] G. Garcia-Belmonte, P. P. Boix, J. Bisquert, M. Sessolo, and H. J. Bolink, Sol. Energy Mater. Sol. Cells **94**, 366 (2010).
[49] G. Juska, G. Sliauzys, K. Genevicius, K. Arlauskas, A. Pivrikas, M. Scharber, G. Dennler, N. S. Sariciftci, and R. Österbacka, Phys. Rev. B **74**, 115314 (2006).
[50] A. J. Mozer, G. Dennler, N. S. Sariciftci, M. Westerling, A. Pivrikas, R. Österbacka, and G. Juska, Phys. Rev. B **72**, 035217 (2005).
[51] C. Arndt, U. Zhokhavets, M. Mohr, G. Gobsch, M. Al-Ibrahim, and S. Sensfuss, Synth. Met. **147**, 257 (2004).
[52] C. G. Shuttle, B. O'Regan, A. M. Ballantyne, J. Nelson, D. D. C. Bradley, J. de Mello, and J. R. Durrant, Appl. Phys. Lett. **92**, 093311 (2008).
[53] D. Schroder, Semiconductor Material and Device Characterization (Wiley-IEEE Press, Hoboken, 2006), p. 391.
[54] A. Maurano, R. Hamilton, C. G. Shuttle, A. M. Ballantyne, J. Nelson, B. O'Regan, W. Zhang, I. McCulloch, H. Azimi, M. Morana, C. J. Brabec, and J. R. Durrant, Adv. Mater. **22**, 49872 (2010).
[55] R. S. Crandall, J. Appl. Phys. **54**, 7176 (1983).
[56] C. Hof, N. Wyrsch, and A. Shah, J. Non-Cryst. Solids **266–269**, 1114 (2000).
[57] J. Merten, J. M. Asensi, C. Voz, A. V. Shah, R. Platz, and J. Andreu, IEEE Trans. Electron Devices **45**, 423–429 (1998).
[58] K. Taretto, U. Rau, and J. H. Werner, Appl. Phys. A **77**, 865–871 (2003).
[59] H. Okamoto, H. Kida, S. Nonomura, K. Fukumoto, and Y. Hamakawa, J. Appl. Phys. **54**, 3236 (1983).
[60] T. Tiedje, Appl. Phys. Lett. **40**, 627 (1982).
[61] F. Monestier, J.-J. Simon, P. Torchio, L. Escoubas, F. Flory, S. Bailly, R. de Bettignies, S. Guillerez, and C. Defranoux, Sol. Energy Mater. Sol. Cells **91**, 405 (2007).